Research Square

Preprints are preliminary reports that have not undergone peer review.
They should not be considered conclusive, used to inform clinical practice,
or referenced by the media as validated information.

Effect of ultrasonic impact treatment on microstructure and properties of Ti6Al4V titanium alloy manufactured by laser directed energy deposition

Jiaqi Li
Nantong University
Xiaofeng Wan
Nantong University
Jinchao Zhang
zhangjc@ntu.edu.cn
Nantong University https://orcid.org/0009-0006-3863-9311
Boyong Su
Nantong University
Yongfei Yang
Nantong University

Research Article

Keywords: Laser directed energy deposition, Ultrasonic impact treatment, Ti6Al4V coatings, Wear resistance, Corrosion resistance

Posted Date: July 24th, 2026

DOI: https://doi.org/10.21203/rs.3.rs-10039191/v1

License: This work is licensed under a Creative Commons Attribution 4.0 International License.
Read Full License

Effect of ultrasonic impact treatment on microstructure and properties of Ti6Al4V titanium alloy manufactured by laser directed energy deposition

Jiaqi Li[a], Xiaofeng Wan[a,*], Jinchao Zhang[a,b,c,*], Boyong Su[a], Yongfei Yang[a]

[a]*School of Mechanical Engineering, Nantong University, Nantong 226019, China*

[b]*School of Optoelectronic Science and Engineering, Soochow University, Suzhou 215021, China*

[c]*Nantong Dart-Rich Fan Co., LTD, Nantong 226019, China*

Corresponding authors: zhangjc@ntu.edu.cn (Jinchao Zhang)

Abstract: To optimize the performance of Ti6Al4V coatings fabricated by laser directed energy deposition (LDED), ultrasonic impact treatment (UIT) was adopted for surface strengthening. In this study, the effects of ultrasonic impact power on the surface roughness, phase composition, microstructure, wear resistance, and corrosion resistance of the Ti6Al4V coating were investigated. The results show that UIT process does not change the phase composition of the Ti6Al4V cladding layer but effectively improves the surface quality by reducing surface waviness and burrs. The UIT process can refines the grains, and the grain refinement becomes more pronounced with increasing UIT power. Regarding performance enhancement, compared with the untreated Ti6Al4V cladding layer, UIT significantly improves the wear resistance. The friction coefficient and wear rate of the 1000 W UIT-treated layer are remarkably reduced, which is primarily attributed to grain boundary strengthening from grain refinement and the dense plastic deformation strengthening layer formed on the surface. Furthermore, the corrosion resistance of cladding layer is synchronously improved, with its corrosion potential (Ecorr) increasing from -0.663 V vs. SCE of the untreated sample to -0.530 V vs. SCE of 1000 W UIT-treated sample.

Keywords: Laser directed energy deposition; Ultrasonic impact treatment; Ti6Al4V coatings; Wear resistance; Corrosion resistance

1. Introduction

Ti6Al4V alloy, as a typical dual-phase (α+β) titanium alloy, is widely used in key components in the aerospace field such as airframe frames, aeroengine compressor blades, and spacecraft structural parts due to its excellent mechanical stability, high specific strength, and corrosion resistance [1-3]. Under extreme conditions, these components are prone to damage, and the repair and remanufacturing of such high-value components can significantly improve economic benefits and resource utilization efficiency [4, 5].

Laser directed energy deposition (LDED) [6, 7], as a metal additive

manufacturing technology, provides an innovative solution for the repair of high-value and difficult-to-process components, especially suitable for performance-matched repair of complex structural parts. Wang et al. [8] successfully fabricated Ti6Al4V coatings using LDED. They pointed out that the incorporation of B_4C particles into Ti-based coatings can enhance the resistance to plastic deformation, high-temperature wear resistance, and microhardness, thereby improving the reliability and service life of component repair. Chen et al. [9] also successfully prepared in-situ synthesized TiC-reinforced Ti6Al4V matrix composite coatings via LDED. Experimental results showed that the coating was uniform and dense, with no obvious defects, and formed a good metallurgical bond with the substrate. The wear resistance, corrosion resistance, and cavitation erosion resistance were all significantly enhanced, which enabled the composite coating to exhibit broader potential application in flow passage components. In order to improve the structure and performance of materials produced by additive manufacturing, optimizing process parameters is a common method. Lu et al. [10] investigated the effect of LDED process on the mechanical properties and corrosion resistance of Ti6Al4V by varying laser power and scanning speed. The results indicated that the Ti6Al4V alloy with excellent comprehensive properties can be obtained through process regulation. Xiao et al. [11] explored the influence of solid solution temperature on the microstructure and mechanical properties of LDED-prepared refractory high-entropy alloys. They found that the sample subjected to solid solution temperature at 1000°C exhibited the optimal matching of strength and toughness, and the underlying intrinsic strengthening mechanism was elucidated. However, there are inherent limitations in only optimizing the laser process. Firstly, columnar grains are still remained in the laser-deposited samples, which leads to an imbalance of mechanical properties. Furtherfore, the high tensile residual stress will be produced by the non-equilibrium solidification and periodic evolution of the temperature field in the LDED process, which has a significantly adverse effect on fatigue performance. In addition, the surfaces and contact interfaces of key components, such as aeroengine compressor disks and blade tenons, are prone to wear and crack initiation under high load and thermal cycling. Therefore, surface strengthening treatment is required for the additive repair/remanufacturing of such components to extend their service life [12].

The surface strengthening treatment for metal material is a commonly used technology to improve key surface properties such as hardness, wear resistance, and

corrosion resistance, as well as to extend service life. Zhang et al. [13] adopted layer-by-layer shot peening (SP) on FeCrNiBSi alloys manufactured by LDED, and the similarities and differences in mechanical properties and microstructure between the hybrid process and traditional LDED were compared. The results showed that the hybrid process of LDED and SP significantly improved the yield strength, ultimate tensile strength, and average hardness of the formed samples. The coarse columnar grains were refined, and the heterogeneity of grain size was reduced. Sapam et al. [14] employed laser shock peening (LSP) for the post-processing of the LDED-prepared Ti6Al4V deposits. The results indicated that LSP treatment significantly improved the fatigue life of the samples and shorten the manufacturing time. Li et al. [15] performed ultrasonic impact treatment (UIT) on LDED-prepared IN718 superalloys. By optimizing the UIT process parameters, the surface microstructure and residual stress distribution were effectively regulated, and the synergistic enhancement of strength and ductility was achieved. Liu et al. [16] pointed out that the recrystallization during the deposition contributed to grain refinement of LDED Ti6Al4V alloys. Generally speaking, the hybrid processing method of additive manufacturing and post-processing can effectively refine grains through the recrystallization process, which leads to significant enhancement of mechanical properties. However, current research on the correlation between process parameters and structure-performance of such hybrid processing methods is limited, and further verification is required for their industrial application.

In this study, Ti6Al4V cladding layers were prepared by LDED and then treated by UIT. Through comprehensive investigations on the surface roughness, microstructure, phase composition, wear resistance, and corrosion resistance of the cladding layers, the optimal UIT power parameters were determined. This work provides valuable references for the application of UIT technology in regulating the properties of Ti6Al4V coatings.

2. Experimental procedure

In this study, Ti6Al4V plates with dimensions of 120 mm × 120 mm × 8 mm were used as the substrate, and spherical Ti6Al4V alloy powders with a particle size distribution of 53-150 μm were selected as the deposition feedstock. The chemical composition of the Ti6Al4V powders is presented in Table 1. Prior to LDED experiments, preprocessing was performed: the powders were dried for 2 h in a vacuum oven at 120°C, and the substrate was polished and cleaned with acetone,

sandpaper, and anhydrous ethanol. The experimental setup consisted of an LDED system and an UIT system, as shown in Fig. 1. The LDED equipment was mainly composed of a laser heat source with a maximum output power of 6 kW, a numerically controlled workbench, a powder feeder, a coaxial powder deposition head, and a gas shielding device. The UIT equipment (HY25-50G) comprised an ultrasonic transducer, an amplitude transformer, and an ultrasonic probe. The configuration of the UIT system is schematically illustrated in Fig. 1(b), where the impact pin strikes the horizontal surface and moves along a "Z"-shaped path perpendicular to the laser cladding direction. Detailed process parameters for Ti6Al4V coating preparation are listed in Table 2. This study focused on investigating the effect of UIT power, with five power levels set: 0 W, 400 W, 600 W, 800 W, and 1000 W, denoted as U0, U4, U6, U8, and U10 respectively. After coating preparation, the coatings were cut into small specimens of 10 mm × 10 mm × 8 mm using a precision wire-cutting method. The metallographic samples were grinded with #600, #800, #1000, #1200, #1500, and #2000 SiC sandpaper, and polished with a 2.5 μm diamond suspension. They were then rinsed with deionized water and absolute ethanol, and dried in a desiccator at room temperature.

The phase composition of the coatings was analyzed via X-ray diffraction (XRD, Ultima IV) using a Cu target (λ = 0.15406 nm) under the microscale mode. A confocal microscope (μsurf mobile) was employed to measure the surface morphology of the samples. To ensure measurement accuracy, the surface roughness was evaluated three times independently, and the average value was used as a reliable indicator for surface roughness assessment. An etchant was prepared with a mass-volume ratio of 2HF + $4HNO_3$ + $100H_2O$, and the etching time was controlled between 38 s and 45 s. After etching, the grain size, micro-morphology, and area distribution were analyzed using a metallographic microscope (MR2100) and a field-emission scanning electron microscope (SEM, GeminiSEM300). The friction and wear properties of the surface-treated samples were tested using a multifunctional friction and wear tester (MFT-5000) under the conditions of a 20 N load, 2 Hz frequency, and 30 min test duration. The volume and morphology of wear scars were measured using a confocal microscope (μsurf mobile). Electrochemical tests were conducted using an electrochemical workstation (CHI660C) with a three-electrode system. The coated alloy with an exposed area of 1 cm^2 served as the working electrode, a Pt electrode as the counter electrode, and a saturated calomel electrode (SCE) as the reference

electrode. In a 3.5 wt% NaCl solution, the open-circuit potential (OCP) was recorded using the electrochemical workstation for 230 s. Subsequently, electrochemical impedance spectroscopy (EIS) was performed at the open-circuit potential. For the potentiodynamic polarization test, the scan rate was set to 10 mV/s, and the scan potential range was from −1 V (vs OCP) to 1.3 V (vs SCE). All electrochemical tests were carried out at room temperature, and each test was repeated at least three times under the same conditions to ensure the accuracy of the results.

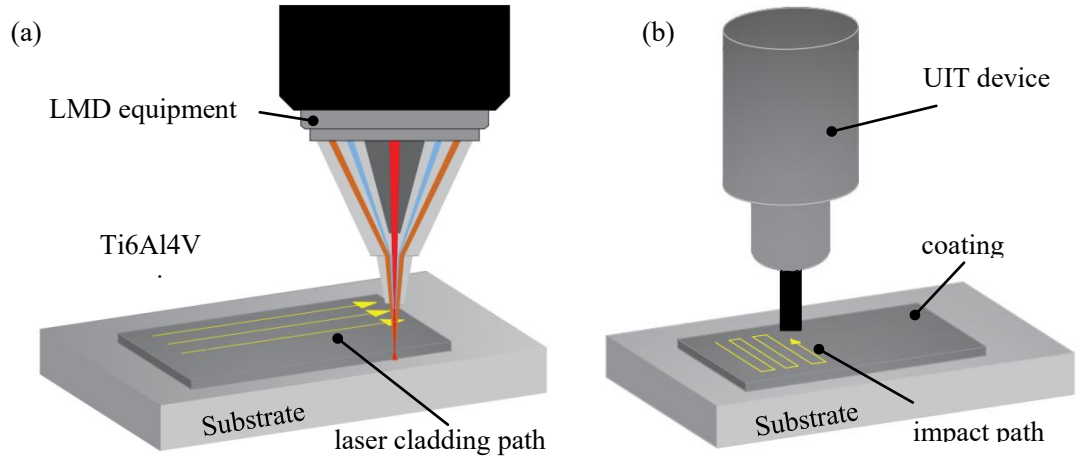

Fig. 1. Schematic illustration of sample preparation. The main setups of (a) laser directed energy deposition (LDED) and (b) ultrasonic impact treatment (UIT) techniques.

Table 1 Chemical composition of Ti6Al4V powder.

Element	V	Al	Fe	O	N	H	C	Ti
Wt.%	3.88	6.06	0.024	0.059	0.0088	0.0012	0.0073	Bal.

Table 2 Process parameters for Ti6Al4V coating.

Laser power (kW)	Scanning speed (mm/s)	Powder feed rate (r/min)	Shielding gas (L/min)	Overlap rate (%)	Impact frequency (kHz)
2.2	14	0.8	20	50	20

3. Results and discussion

3.1. Macrostructure and microstructure characteristics

Fig. 2 shows the surface topography of the laser-deposited samples after ultrasonic impact treatment (UIT) at varying power levels. The as-fabricated sample exhibites pronounced undulations and burrs (Fig. 2(a)). Following UIT, these surface irregularities are substantially diminished, resulting in a smoother surface (Fig. 2(b-e)). Fig. 3(a) shows the cross-sectional profile of samples at different powers. It demonstrates that the height of groove structures decreases significantly with increasing power, which is consistent with the above observations. It can be seen from

Fig. 3(b), compared to the untreated sample (U0), the surface roughness of samples is reduced by 13.9%, 29.8%, and 36.4% respectively when the UIT power of 400 W (U4), 600 W (U6) and 800 W (U8) is used. However, when the UIT power is increased to 1000 W (U10), the surface roughness reduction decreases to 33.4%, which implies that excessive UIT power may induce surface damage and lead to a marginal increase in surface roughness. It is noteworthy that the surface undulations introduced by UIT are significantly smaller than those caused by conventional surface strengthening techniques [17, 18], ensuring a negligible impact on dimensional accuracy while maintaining excellent surface integrity.

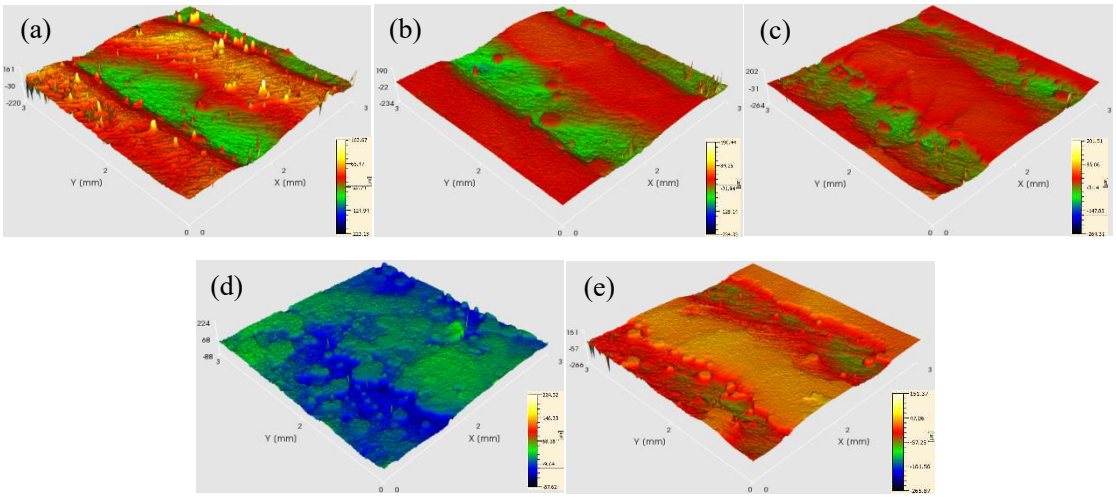

Fig. 2. 3D surface morphologies of the laser-deposited samples under different ultrasonic impact powers: (a) U0, (b) U4, (c) U6, (d) U8 and (e) U10.

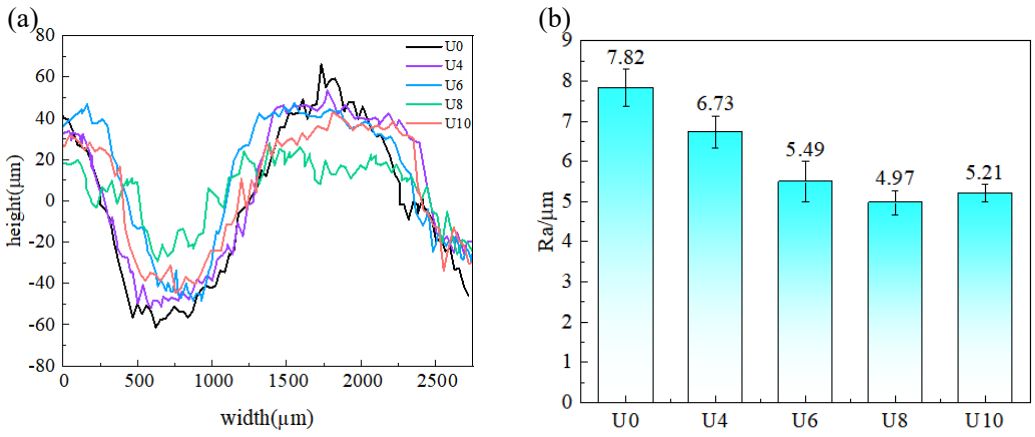

Fig. 3. (a) 2D contour of samples at different powers, (b) the surface roughness of samples at different powers.

Fig. 4 displays the XRD patterns of Ti6Al4V samples under different UIT powers. As illustrated in Fig. 4(a), the diffraction peaks of the as-deposited sample are predominantly indexed to the hexagonal close-packed (hcp) α/α′ martensitic phases. Owing to the identical crystal structure between the non-equilibrium α′ martensite and

the α phase, their diffraction peaks are completely overlapped. After UIT, the phase constituents remain unchanged. No distinct diffraction peaks corresponding to the body-centered cubic (bcc) β phase are detected, which can be attributed to the coarse millimeter-sized columnar β grains failing to provide sufficient diffraction intensity.

Fig. 4(b) shows the normalized diffraction peaks of the α/α′ martensite for the (100), (002), and (101) planes. With increasing UIT power, the diffraction peaks shift systematically toward higher angles, indicating the introduction of considerable compressive residual stresses [19, 20]. Concurrently, progressive peak broadening is observed with higher UIT power. It suggests that the treatment induces grain refinement, lattice distortion, and an increase in microstrain within the surface layer [21]. Furthermore, the as-deposited sample exhibits a significantly stronger α/α′ (110) diffraction peak compared to other characteristic peaks. As the UIT power increases, the intensity of the α/α′ (110) peak gradually decreases, while the α/α′ (101) peak shows a relative enhancement. This phenomenon indicates that the strong pre-existing (110) solidification texture in the near-surface region is notably disrupted or weakened due to UIT, resulting in a reduced diffraction intensity along the (110) orientation and a concomitant increase in the (101) diffraction signal.

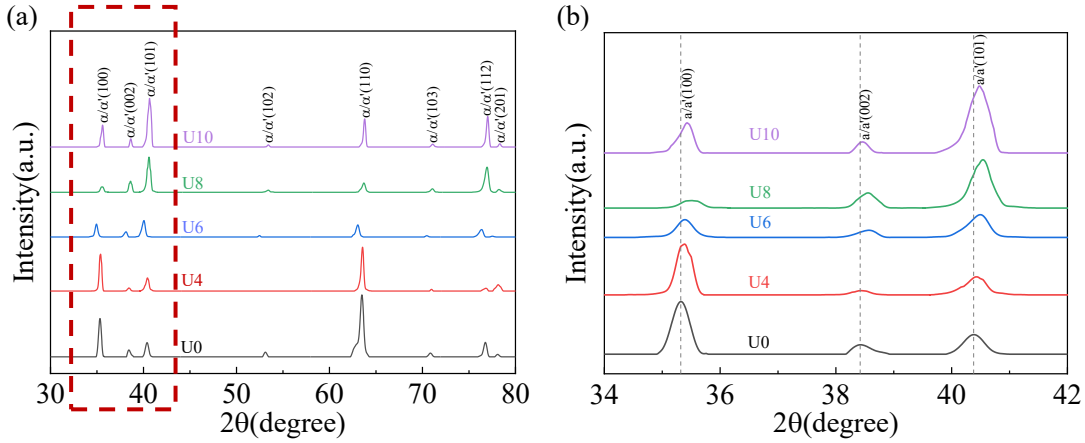

Fig. 4. (a) XRD patterns of the different coatings, (b) an enlarged view of the red box in Fig. 4(a).

Fig. 5 presents the microstructural evolution of cross-sections of LDED specimens without ultrasonic impact and under different ultrasonic impact powers via optical microscopy (OM) and scanning electron microscopy (SEM). OM images indicate that all specimens exhibit the typical characteristics of LDED. The macrostructures are dominated by columnar β grains, which grow along the building direction. For the U0 group without UIT (Fig. 5(a)), the columnar β grains grow adequately with coarse size and clear grain boundary contours. From Fig. 5(c, e, g, i),

the grain refinement effect is significant after UIT. It can be attributed to the plastic deformation and dynamic recrystallization. As the ultrasonic impact power increases from 400 W to 1000 W, the width of columnar β grains decreases continuously and the grain boundaries become gradually blurred. This phenomenon originates from the synchronous enhancement of impact mechanical intensity and vibration energy density under higher power. The stronger impact load intensifies the accumulation of plastic deformation storage energy, while higher vibration energy accelerates the dynamic recrystallization kinetics. The synergistic effect of the two remarkably inhibits the directional growth tendency of columnar grains, realizing gradient grain refinement.

The slender acicular structures are observed within β grains. Combined with the phase transformation characteristics of Ti6Al4V alloy of laser cladding, this acicular structure is identified as α′ phase [22]. In Fig. 4(b), the β grains contain typical dense slender acicular α′ phases, which are oriented parallel or perpendicular to each other [23]. After applying ultrasonic impact, with the increase of power, the interior of β grains gradually transforms from an α′ phase-dominated acicular structure to a basket-weave structure coexisting with α phase (laths with increased width) and residual α′ phase [24,25].

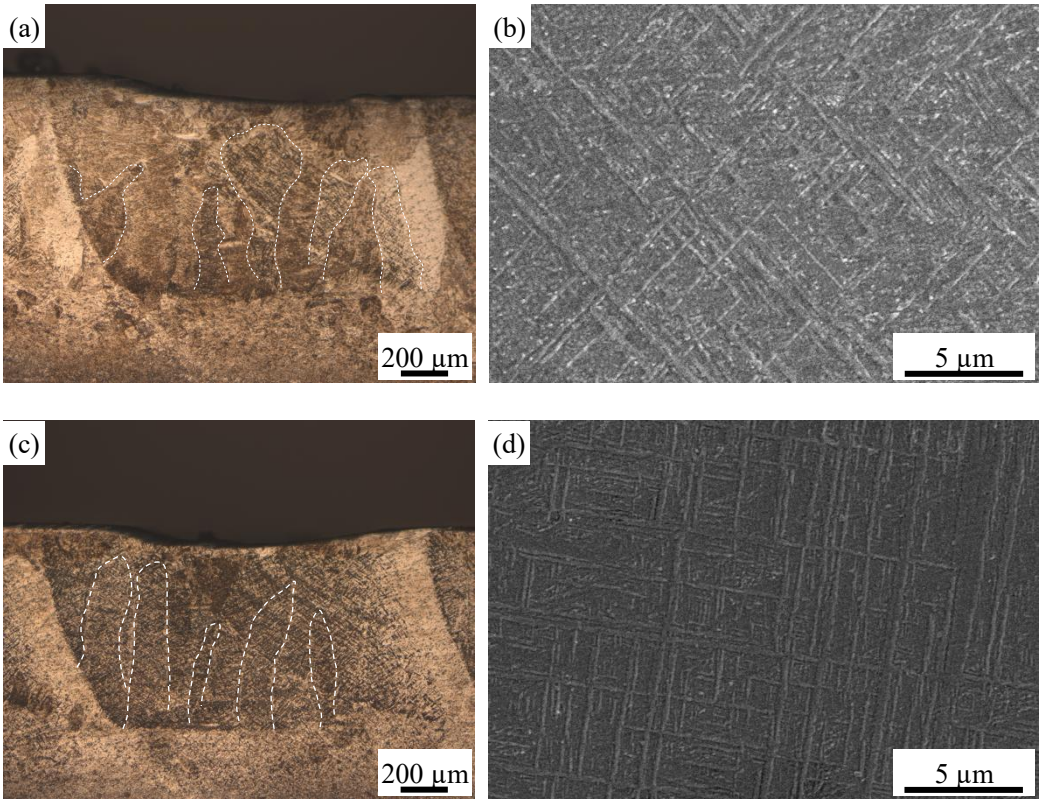

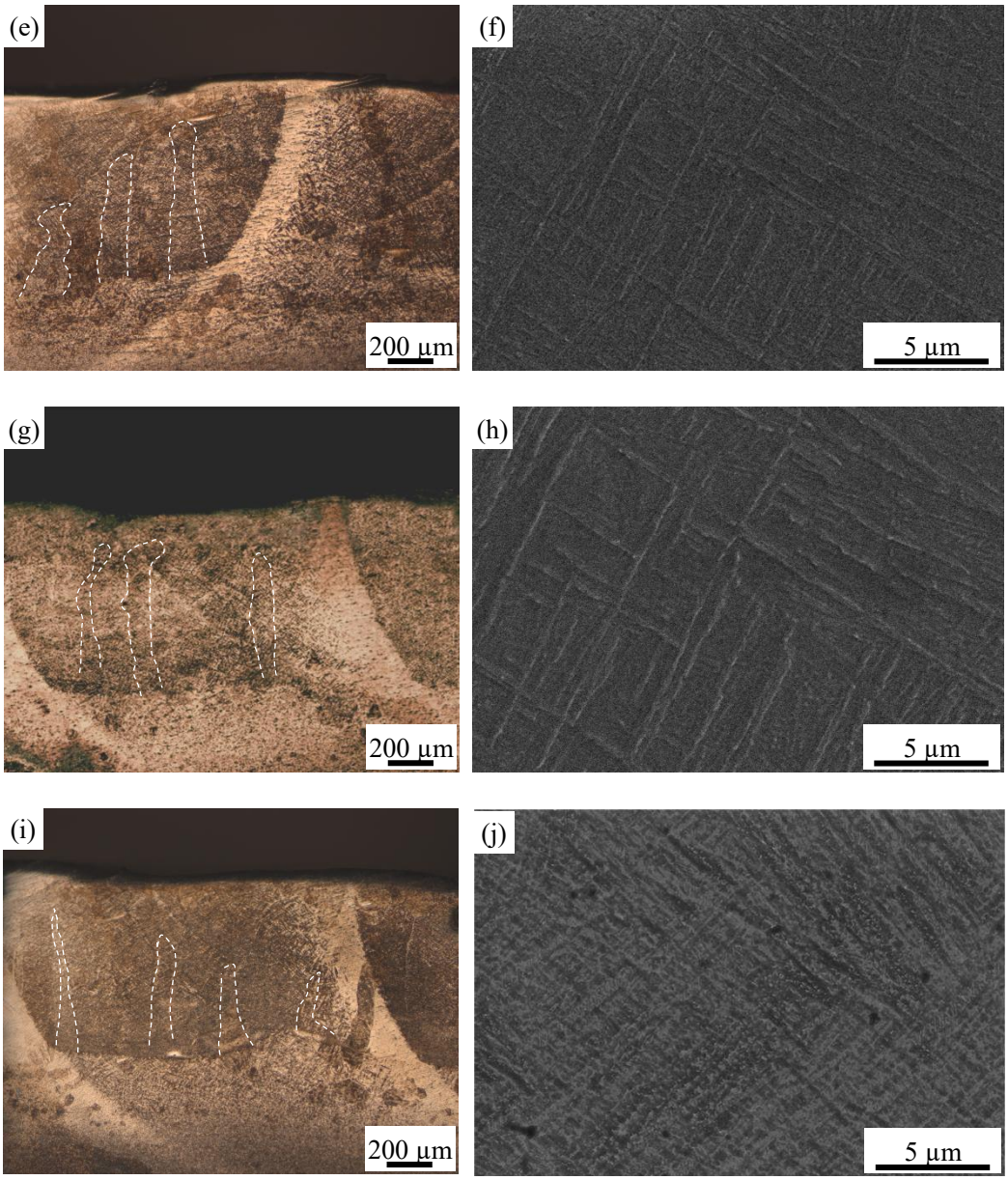

Fig. 5. Microstructure of samples under different ultrasonic impact power: (a, b) U0, (c, d) U4, (e, f) U6, (g, h) U8, and (i, j) U10.

3.2. Wear resistance

In tribological studies, the friction coefficient is a fundamental parameter for characterizing material behavior. It is a key index to quantify the interaction between surfaces during mechanical contact and wear processes [26]. The relationship between ultrasonic impact power and frictional behavior is presented in Fig. 6(a). Typically, the friction coefficient undergoes an initial transition period before stabilizing. It can be observed that within the first 1 minute, the coating exhibits a sharp increase in friction value with significant instability. As time progresses, the surface flattening reduces local stress, allowing the system to transition to a steady-state wear stage with

diminished friction fluctuations [27-29]. Variations in UIT power induce notable changes in the friction coefficient. The friction coefficient of the LDED sample (U0) is approximately 0.2216, and the friction coefficient decreases remarkably to below 0.2143 when UIT process is applied. With the further increase of UIT power, the friction coefficient decreases gradually, and it drops to 0.1917 at a power of 1000 W. Based on the friction coefficient results, it is preliminarily concluded that the Ti6Al4V cladding layer has the best wear resistance when the ultrasonic impact power is 1000 W.

To further explore the wear resistance of Ti6Al4V cladding layers under different ultrasonic impact powers, the wear mass loss under various powers was measured, as shown in Fig. 6(b). The wear mass loss of the LDED sample is 0.7 mg. After ultrasonic impact is applied, the wear loss decreases significantly. At the ultrasonic powers of 600 W and 800 W, the wear mass loss values are approximately 0.4 mg and 0.39 mg, respectively. When the ultrasonic power is 1000 W, the wear mass loss reaches the minimum value of about 0.3 mg.

To better illustrate the differences in wear resistance, the wear rate of Ti6Al4V cladding layers under different ultrasonic impact powers was calculated using Equation (1):

$$\delta = \frac{V}{\sum W} \tag{1}$$

Here, V represents the wear volume of the specimen, and $\sum W$ denotes the cumulative friction work, which can be expressed as the product of the normal load and the wear distance [30]. The calculated wear rates corresponding to different conditions are shown in Fig. 6(c), and it can be seen that the variation of wear rate is consistent with that of wear mass loss, with specific values of 1.44, 1.31, 1.13, 1.11, and 0.847 $mm^3/(N \cdot m)$. According to the trend of wear rate, the lower the wear rate, the better the wear resistance. Therefore, it can be inferred that the Ti6Al4V cladding layer shows the optimal wear resistance at an impact power of 1000 W, which is consistent with the observed trend of wear mass loss.

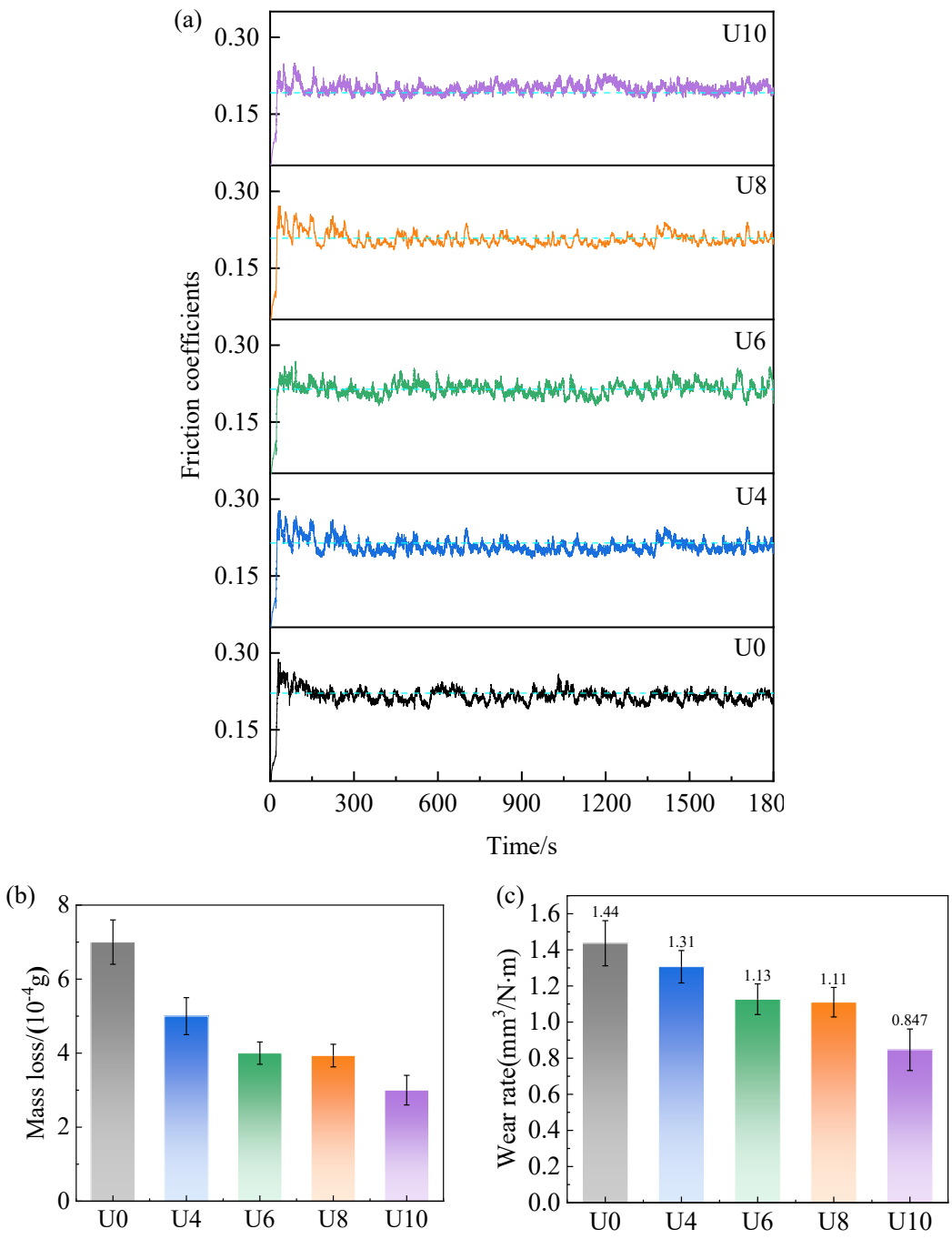

Fig. 6. (a) Friction coefficient curves, (b) mass loss and (c) wear rate.

Fig. 7 and Fig. 8 respectively demonstrate the three-dimensional (3D) and two-dimensional (2D) wear scar morphologies of Ti6Al4V cladding layers under different ultrasonic impact powers. It can be clearly seen from Fig. 7 that the wear scars under different UIT powers generally exhibit plough-like groove characteristics. From Fig. 8, it shows that a deep and obvious groove for the LDED sample (U0) is formed, and the wear depth is about 24.5 μm. After applying ultrasonic impact treatment, the wear depth decreases significantly. The wear depth of the U4 sample has decreased obviously, and when the UIT power is increased to 600 W and 800 W,

the wear depth continues to decrease, and the wear track becomes smoother. Notably, at the UIT power of 1000 W, the wear depth reaches the minimum value, about 4.7 μm. The wear scar morphology is relatively uniform and smooth compared with the samples treated at low power. Thus, the 1000 W ultrasonic impact treatment can effectively improve the wear resistance of Ti6Al4V cladding layers by reducing the wear depth and optimizing the surface integrity.

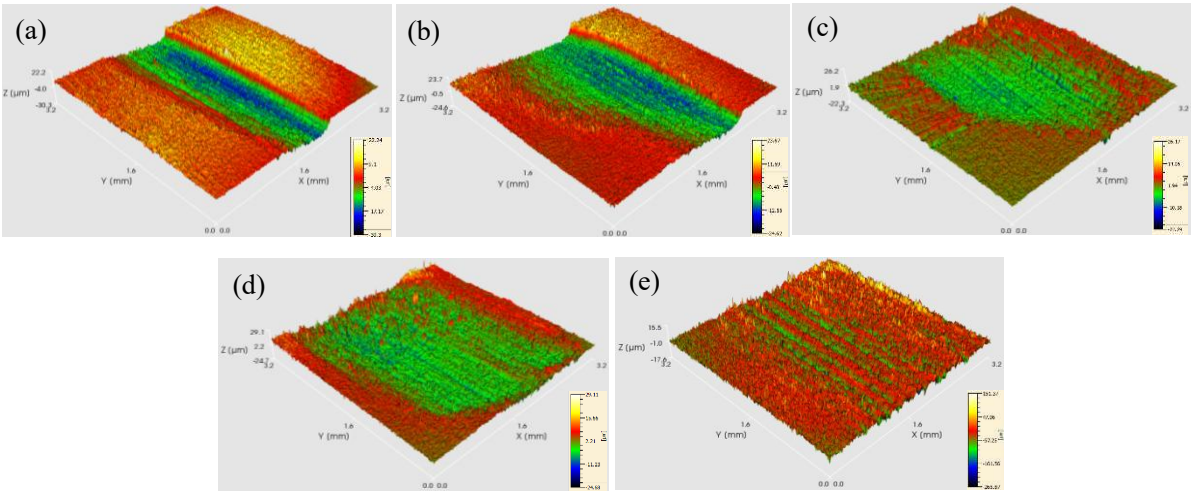

Fig. 7. 3D wear patterns under different UIT powers: (a) U0, (b) U4, (c) U6, (d) U8, and (e) U10.

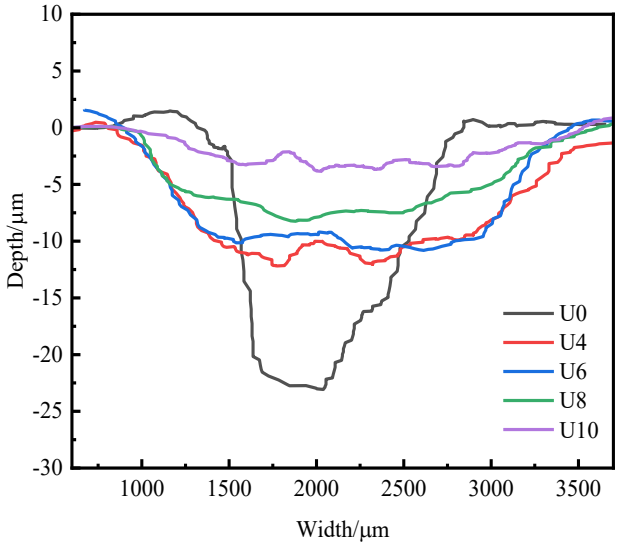

Fig. 8. 2D wear scar morphologies under different UIT powers.

3.3. Corrosion resistance

Fig. 9(a) displays the potentiodynamic polarization curves of the laser-deposited samples at different UIT powers. It can be observed that the polarization curves under different UIT powers exhibit similar overall shapes. The cathodic branches show no significant differences in trend, indicating that the cathodic reaction mechanism remains consistent across all samples, though occurring at varying rates. Furthermore,

all specimens demonstrate distinct passivation behavior. It is confirmed that a protective passive film is formed in the NaCl solution, which can effectively inhibit the further corrosion of the alloy.

The corrosion potential (E_{corr}) and corrosion current density (I_{corr}), derived from fitting the polarization curves, are summarized in Table 3. E_{corr} reflects the thermodynamic tendency of the material to corrode, while I_{corr} represents the kinetic rate of corrosion. Compared to the untreated laser-deposited sample, all UIT-treated specimens exhibit a positive shift in E_{corr}. This shift becomes more pronounced with increasing UIT power, indicating that higher UIT power enhances the thermodynamic stability of the material surface [31]. Concurrently, the I_{corr} values of UIT-treated samples decrease by approximately an order of magnitude, demonstrating a significant improvement in corrosion resistance. A further slight reduction in I_{corr} is observed with continued increase in UIT power, suggesting additional enhancement of corrosion performance.

Fig. 9(b-d) presents the electrochemical impedance spectroscopy (EIS) of the Ti6Al4V cladding layer under different UIT powers. Fig. 9(b) shows the Nyquist plots at various powers. The size of the capacitive loop in the Nyquist plot is correlated with corrosion resistance. The larger the loop, the higher the corrosion resistance [32]. As observed from the Fig. 9(b), all curves exhibit similar capacitive arc behavior, and the capacitive reactance radius gradually increases with the increase in ultrasonic impact power. At an impact power of 1000 W, the cladding layer achieves the maximum capacitive reactance radius, indicating the optimal corrosion resistance at this power. The enhanced UIT power promotes grain refinement on the cladding surface and reduces defects such as microholes and cracks, which minimizes the penetration channels of corrosive media. Ultimately, this manifests as an increase in capacitive reactance radius and improved corrosion resistance.

Fig. 9(c, d) displays the Bode plots, which characterize the impedance spectroscopy in terms of impedance modulus and phase angle. A higher impedance modulus and phase angle in the low-frequency region of the Bode plot indicate superior corrosion resistance of the material [33]. In the high-frequency region, the impedance amplitude tends to stabilize and form a plateau. This feature implies the electrolyte resistance remains constant and is less affected by frequency variations. Further analysis of the Bode plot in the medium-frequency range reveals a slope close to -1, showing a significant linear characteristic. This phenomenon is a typical

capacitive behavior of the passive film, indicating that the charge storage and release processes dominate. Discrepancies in impedance modulus and phase angle exist among different samples in the low-frequency region, which are associated with the microstructure of the alloy, surface state, and inhomogeneity of the passive film. It can be seen from Fig. 9(c, d) that as the impact power increases, the low-frequency impedance modulus and phase angle gradually increase. Additionally, the U10 sample exhibits the highest impedance modulus and phase angle, as well as the widest phase angle plateau. The most stable passive film is formed. This is because higher ultrasonic impact power strengthens the plastic deformation and grain refinement effects on the cladding surface [34]. It facilitates the uniform distribution of passive film components, and reduces pores and weak areas in the film layer, and thereby enhances the structural stability and corrosion resistance of the passive film. This result is consistent with the conclusions from the previous polarization curve analysis.

In summary, the corrosion resistance of the samples follows the order: U10 > U8 > U6 > U4 > U0. The results indicate that the corrosion resistance of the cladding layer is significantly improved with the increase in ultrasonic impact power.

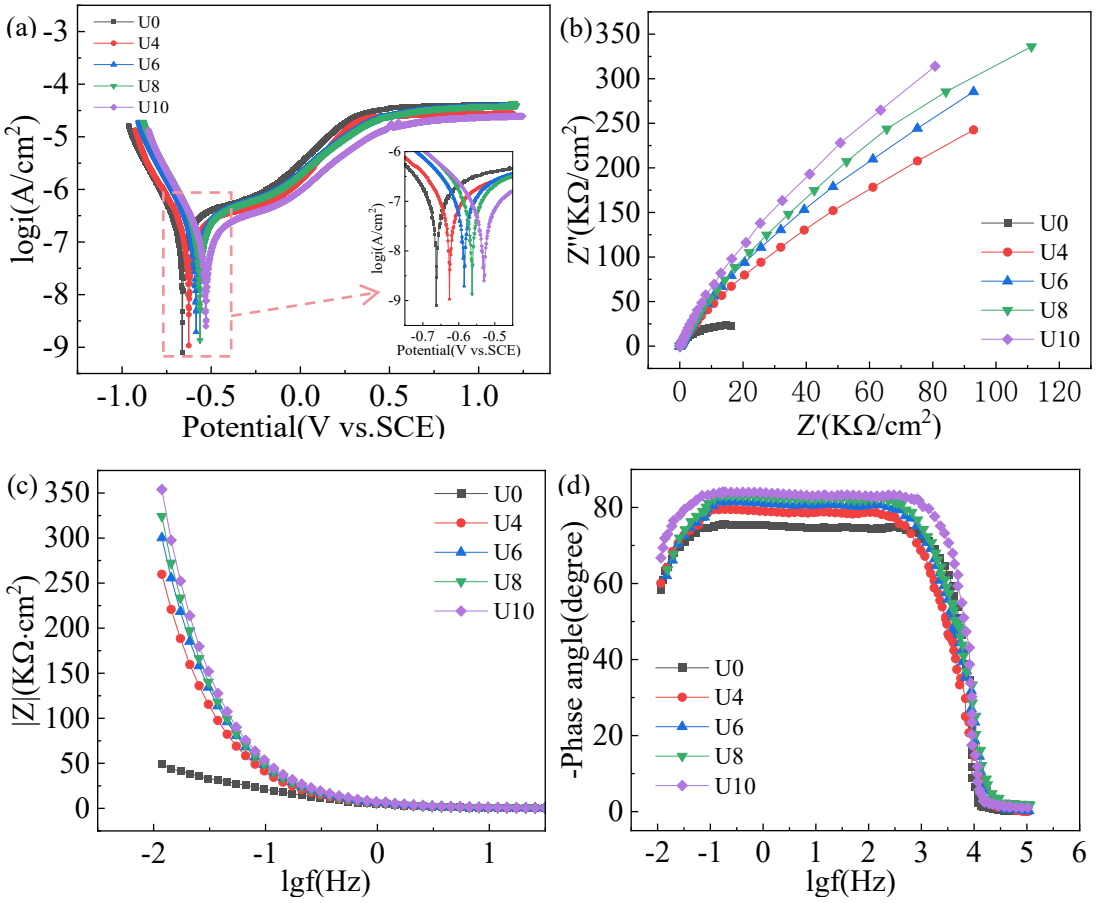

Fig. 9. Corrosion results of the samples: (a) dynamic potential polarization curve plot, (b) Nyquist plot, (c) bode impedance, and (d) bode phase angle.

Table 3 Electrochemical parameters of the samples.

Sample	E_{corr}(V)	I_{corr}(A·cm-2)
U0	-0.663	1.429×10-6
U4	-0.626	1.656×10-7
U6	-0.585	1.495×10-7
U8	-0.563	1.447×10-7
U10	-0.530	1.321×10-7

4. Conclusions

Ti6Al4V cladding layers were fabricated via LDED and subsequently subjected to UIT. The evolution laws of surface roughness, microstructure, phase composition, wear resistance, and corrosion resistance of the cladding layers with respect to ultrasonic impact power were systematically investigated. The optimal ultrasonic impact treatment parameter was determined to be 1000 W, which provides valuable references for the application of UIT in regulating the properties of cladding layers. The main conclusions are as follows:

(1) After UIT, the phase composition of the Ti6Al4V cladding layer remained unchanged, while surface ripples and burrs were significantly reduced, resulting in a smoother surface. UIT effectively refined the grains of the Ti6Al4V cladding layer, breaking down large-sized columnar grains into fine grains. With the increase in ultrasonic impact power, the impact mechanical strength and vibration energy density increased synchronously, leading to a more pronounced grain refinement effect. The further refined grains effectively improved the wear resistance and corrosion resistance of the cladding layer.

(2) UIT significantly enhanced the wear resistance of the Ti6Al4V cladding layer. The friction coefficient decreased from 0.2216 for the U0 sample to 0.1917 for the U10 sample, and the wear rate reduced from 1.44 $mm^3/(N·m)$ (U0) to 0.847 $mm^3/(N·m)$ (U10). The cladding layer treated at 1000 W exhibited the lowest wear rate and friction coefficient, indicating the optimal wear resistance. This is attributed to grain refinement-induced grain boundary strengthening and the formation of a highly dense plastic deformation strengthening layer on the surface.

(3) UIT contributed to the improvement of the corrosion resistance of the Ti6Al4V cladding layer. The corrosion potential of the cladding layer increased from -0.663 V vs. SCE (U0) to -0.530 V vs. SCE (U10). As the ultrasonic impact power increased, the plastic deformation and grain refinement effects on the cladding layer surface were enhanced, which promoted the uniform distribution of passive film

components and reduced pores and weak regions in the film, and consequently improved the structural stability and corrosion resistance of the passive film.

Author Contributions Jiaqi Li contributed to the study conception and design. Material preparation, data collection and analysis were performed by Xiaofeng Wan, Jinchao Zhang, Boyong Su, and Yongfei Yang. The first draft of the manuscript was written by Jiaqi Li and all authors commented on previous versions of the manuscript. All authors read and approved the final manuscript.

Funding This work was supported by the Natural Science Foundation of Jiangsu Province, China (BK20240952), the China Postdoctoral Science Foundation (2025M771391), and the Postgraduate Research & Practice Innovation Program of Jiangsu Province (KYCX25_3699).

Data availability Data and material are completely transparent.

Declarations
Conflict of interest The authors declare no competing interests.

References

1. Perez N, Alvarez-Vera M, Ortega J A, Perez J, Rodriguez Betancourth C A (2025) Tribological and microstructural characterization of laser microtextured Ti-6Al-4V ELI alloy evaluated against UHMWPE and PEEK for biomedical applications. Wear 570:205931
2. Hong D, Zan S, Winter K, Liao Z, Axinte D (2024) On influence of microstructural anisotropy of additive manufactured structures upon machining dynamics: an example of milling of Ti6Al4V thin-walled parts. J. Mater. Process. Technol. 334:118644
3. Huang J, Zhu J, Zhou K, Liu Z, Huang Y. Probing wear mechanism of Ti6Al4V micro-textured surfaces processed by laser-assisted grinding. J. Alloys Compd. 2025;1010:178272
4. Witek L, Bednarz A, Stachowicz F (2015) Fatigue analysis of compressor blade with simulated foreign object damage. Eng. Fail. Anal. 58:229-237
5. Li Y, Chen K, Narayan R L, Ramamurty U, Wang Y, Long J, Tamura N, Zhou X (2020) Multi-scale microstructural investigation of a laser 3D printed Ni-based superalloy. Addit. Manuf. 34:101220
6. Tan C, Weng F, Sui S, Chew Y, Bi G (2021) Progress and perspectives in laser additive manufacturing of key aeroengine materials. Int. J. Mach. Tool Manufact.

170:103804

7. Li Z, Sui S, Ma X, Tan H, Zhong C, Bi G, Clare A T, Gasser A, Chen J (2022) High deposition rate powder- and wire-based laser directed energy deposition of metallic materials: a review. Int. J. Mach. Tool Manufact. 181:103942
8. Wang W L, Zhang K, Liu W J (2025) High-temperature wear resistance of in-situ B_4C particle reinforced TC4 coatings fabricated by laser directed energy deposition. Materials Letters 399:138988
9. Chen H, Yu D T, Mao J T, Wu C L, Zhang S, Zhang C H, Wang Q, Zhang D (2025) Microstructure and tribo-corrosion behavior of TC4 composites reinforced by in situ synthesized TiC ceramics particles through laser cladding. Ceramics International 51:31719-31733
10. Lu X Z, Zou W, Zhou X J, Zhang J, Chen X M, Pang X T, Ip W Y, Lai C P, Chan L C, Wang Y (2025) Effect of process parameters on mechanical properties and corrosion resistance of Ti-6Al-4V alloys prepared by selective laser melting. Journal of Materials Research and Technology 36:1743-1757
11. Xiao B, Li Y, Li S T, Wang A M, Fu H M, Zhang H F, Zhu Z W (2025) The effect of heat treatment on microstructure and mechanical properties of $Ti_3Zr_{1.5}NbVAl_{0.25}$ refractory high entropy alloys fabricated by directed energy deposition. Journal of Materials Research and Technology 39:94-107
12. Lu G, Liu H, Lin C, Zhang Z, Shukla P, Zhang Y, Yao J (2019) Improving the fretting performance of aero-engine tenon joint materials using surface strengthening. Mater. Sci. Technol. 35:1781-1788
13. Zhang X Y, Huang S, Li D C, Geng J L, Yang F, Li Q Y (2022) An approach to improve the microstructure and mechanical properties: a hybrid manufacturing of laser directed energy deposition and shot peening. Additive Manufacturing 55:102686
14. Singha S N, Deogharea A B (2024) Enhanced fatigue performance of laser directed energy deposition fabricated Ti6Al4V alloy using laser shock peening. Procedia Structural Integrity 56:11-18
15. Li Y, Li M Y, Yang H, Dang X F, Cui L Q, Jiao Y, Sun Z P, Guo T, He W F (2025) Enhanced strength-ductility synergy in laser directed energy deposited IN718 superalloys through heterogeneous deformation nanostructures. International Journal of Machine Tools & Manufacture 208:104280
16. Liu Y, Wang F, Xu D, Wang J, Jiang F, Zarinejad M, Tong Y (2023)

Microstructure and mechanical properties of laser metal deposited Ti6Al4V alloy with near equiaxed β grain structure. J. Mater. Res. Technol. 22:1935-1947

17. Lesyk D A, Martinez S, Mordyuk B N, Dzhemelinskyi V V, Lamikiz A, Prokopenko G I (2020) Post-processing of the inconel 718 alloy parts fabricated by selective laser melting: effects of mechanical surface treatments on surface topography, porosity, hardness and residual stress. Surf. Coat. Technol. 381:125136
18. Liu Y G, Li H M, Li M Q (2015) Characterization of surface layer in TC17 alloy treated by air blast shot peening. Mater. Des. 65:120-126
19. Wu A S, Brown D W, Kumar M, Gallegos G F, King W E (2014) An experimental investigation into additive manufacturing-induced residual stresses in 316L stainless steel. Metall. Mater. Trans. 45:6260-6270
20. Lv J, Alexandrov I V, Luo K, Lu H, Lu J (2022) Microstructural evolution and anisotropic regulation in tensile property of cold metal transfer additive manufactured Ti6Al4V alloys via ultrasonic impact treatment. Mater. Sci. Eng. A 859:144177
21. Lesyk D A, Martinez S, Mordyuk B N, Dzhemelinskyi V V, Lamikiz A, Prokopenko G I (2020) Post-processing of the inconel 718 alloy parts fabricated by selective laser melting: effects of mechanical surface treatments on surface topography, porosity, hardness and residual stress. Surf. Coat. Technol. 381:125136
22. Pan X, Zhou L, Wang C, Yu K, Zhu Y, Yi M, Wang L, Wen S, He W, Liang X (2023) Microstructure and residual stress modulation of 7075 aluminum alloy for improving fatigue performance by laser shock peening. Int. J. Mach. Tool Manufact. 184:103979
23. Cao S, Chu R, Zhou X, Yang K, Jia Q, Lim C V S, Huang A, Wu X (2018) Role of martensite decomposition in tensile properties of selective laser melted Ti-6Al-4V. J. Alloys Compd. 744:357-363
24. Zhao Y, Wang M, Lei Y, Fan Y, Xue A, Lin X (2024) Fabrication of heterostructured Ti alloys with exceptional strength and ductility by direct laser deposition. J. Mater. Res. Technol. 28:1597-1610
25. Guo N, Wu D, Yu M, Yin P, Cheng Q, Wang G (2022) Microstructure and properties of Ti-6Al-4V titanium alloy prepared by underwater wire feeding laser deposition. J. Manuf. Process. 73:269-278

26. Wu B, Yang Z, Wang C, Yi J, Yang G (2024) Microstructures and mechanical properties of additive connecting Ti-6.5Al-2Zr-1Mo-1V alloy by high frequency pulse TIG technology. Trans. Indian Inst. Met. 77:4119-4128
27. Ge Y, Cheng J, Zhang B, et al (2022) Sliding wear behaviors of the AlNiTi amorphous coatings: effect of temperatures. J Mater Res Technol 21:2362-2374
28. Blau P J (2001) The significance and use of the friction coefficient. Tribol Int 34(9):585-591
29. Tong Z, Pan X, Zhou W, et al (2021) Achieving excellent wear and corrosion properties in laser additive manufactured CrMnFeCoNi high-entropy alloy by laser shock peening. Surf Coat Technol 422:127504
30. Wu Q, Long W, Zhang L, et al (2024) The microstructure and wear behavior of WC-reinforced diamond composite coating. Weld World 68(7):1685-1692
31. Zhang Y, Liu Z, Wang Y, et al (2025) Study on microstructure and sliding wear behavior of similar and dissimilar welded joints produced by laser-arc hybrid welding of wear-resistant steels. Wear 562-563:205643
32. Shokouhfar M, Allahkaram S R (2017) Effect of incorporation of nanoparticles with different composition on wear and corrosion behavior of ceramic coatings developed on pure titanium by micro arc oxidation. Surface & Coatings Technology 309:767-778
33. Dai N, Zhang J, Chen Y, Zhang L C (2017) Heat treatment degrading the corrosion resistance of selective laser melted Ti-6Al-4V alloy. J Electrochem Soc 164:C428-C434
34. Zhou S, Zhao Y, Wang X, Li W, Chen D, Sercombe T B (2020) Enhanced corrosion resistance of Ti-5 wt.% TiN composite compared to commercial pure Ti produced by selective laser melting in HCl solution. J Alloys Compd 820:153422